RENAL FAILURE
2026, VOL. 48, NO. 1, 2667130
https://doi.org/10.1080/0886022X.2026.2667130

Taylor & Francis
by informa

CLINICAL STUDY

OPEN ACCESS Check for updates

Identification of pyroptosis-related hub genes and immune cell infiltration in IgA nephropathy via bioinformatics analysis

Jiayi Li[a,b], Cheng Zhou[b], Shunlai Shang[b], Qianqian Xu[b] and Wenge Li[a,b]

[a]Department of Nephrology, Peking University China-Japan Friendship School of Clinical Medicine, Beijing, China; [b]Department of Nephrology, China-Japan Friendship Hospital, Beijing, China

ABSTRACT

This study aimed to identify pyroptosis-related hub genes and investigate immune cell infiltration in IgA nephropathy (IgAN) using bioinformatics and experimental validation. Gene expression data from the GEO database (GSE93798) were analyzed, and differential expression analysis was performed using the limma R package. LASSO regression and SVM algorithms were employed to select feature genes. A total of 19 pyroptosis-related differentially expressed genes (nine up-regulated and 10 down-regulated) were identified, with six hub genes (BHLHE40, JUN, CEBPB, ACE2, IL1B, and CD14) showing high diagnostic accuracy for discriminating IgAN from normal samples (AUC > 0.9). Gene Ontology (GO) and KEGG analyses revealed involvement in immune response, cell migration, and inflammation-related signaling pathways. Immune cell infiltration analysis showed higher levels of CD8+ T cells, macrophages, and neutrophils in IgAN. Validation using GSE99339 confirmed these findings, with the hub genes also demonstrating high AUC values in this independent dataset. The differential expression of these genes was validated in both human kidney tissues and serum samples. This study provides potential biomarkers and therapeutic targets for IgAN by elucidating pyroptosis-related genes and immune cell infiltration profiles.

ARTICLE HISTORY
Received 6 July 2025
Revised 8 January 2026
Accepted 20 March 2026

KEYWORDS
IgA nephropathy; pyroptosis; bioinformatics; immune cell infiltration; hub genes

1. Introduction

IgA nephropathy (IgAN) is one of the most common causes of chronic kidney disease (CKD) worldwide, characterized by the deposition of IgA-containing immune complexes in the glomerular mesangium [1,2]. Despite extensive research into its clinical and pathological features, the underlying molecular mechanisms driving IgAN remain poorly understood [3,4]. Current therapeutic strategies for IgAN primarily rely on nonspecific supportive treatments, such as optimal blood pressure control and reduction of proteinuria through renin–angiotensin–aldosterone system (RAAS) blockade [5]. However, these non-targeted therapies offer limited efficacy, and many patients continue to progress to end-stage renal disease (ESRD) despite optimized management [6]. Therefore, there is an urgent need to identify novel molecular targets and develop more effective therapeutic approaches for IgAN.

Pyroptosis is a recently recognized form of programmed cell death associated with inflammation, and it plays a critical role in the pathogenesis of various inflammatory and autoimmune diseases. This process involves the activation of inflammasomes and gasdermin family proteins, resulting in cell membrane rupture and the release of pro-inflammatory cytokines. Key pyroptosis-related molecules, such as NOD-like receptor family pyrin domain containing 3 (NLRP3), gasdermin D (GSDMD), gasdermin E (GSDME), and caspases 1, 3, and 11, have been implicated in acute and CKD models. In IgAN, IgA immune complexes have been shown to activate the NLRP3 inflammasome in macrophages and podocytes [7,8]. Moreover, elevated levels of IL-1β and IL-18, hallmark cytokines of inflammasome activation, have been observed in patients with IgAN [9,10]. Tsai et al. reported that NLRP3 activation contributes to disease progression

CONTACT Wenge Li liwenge@pumc.edu.cn Department of Nephrology, Peking University China-Japan Friendship School of Clinical Medicine, Beijing, China; Qianqian Xu Xqq816926@163.com Department of Nephrology, China-Japan Friendship Hospital, Beijing, China
Supplemental data for this article can be accessed online at https://doi.org/10.1080/0886022X.2026.2667130.

via T cell activation and mitochondrial reactive oxygen species (ROS) production and that its inhibition can ameliorate IgAN pathology [8].

These findings suggest that pyroptosis-related signaling pathways may represent promising therapeutic targets in IgAN. However, the role of pyroptosis-related genes in the pathogenesis of IgAN remains largely unexplored.

In this study, we employed a comprehensive bioinformatics approach to identify pyroptosis-related hub genes and evaluate immune cell infiltration in IgAN. We analyzed transcriptomic data from the Gene Expression Omnibus (GEO) database, conducted differential expression and enrichment analyses, selected feature genes, and validated our findings using immunofluorescence staining. This study aims to provide new insights into the molecular mechanisms underlying IgAN and to identify potential biomarkers and therapeutic targets for this disease (Figure 1).

2. Methods

2.1. Data acquisition and preprocessing

In this study, gene expression data were downloaded from the GEO database, with the dataset accession number GSE93798. This dataset includes 20 IgAN patient samples and 22 healthy control samples, providing gene expression information related to IgAN. The raw data in the dataset comprised probe matrix files and platform files. We first annotated the probes with gene names based on the platform file annotations and converted the probe matrix into a gene expression matrix for subsequent analysis. All data underwent normalization to eliminate potential batch effects. The limma R package's normalizeBetweenArrays function was used for normalization to ensure data comparability. The ComBat method was employed for batch effect correction to ensure comparability between data from different experimental batches. Principal component analysis (PCA) was performed to visually compare the data before and after batch correction to verify the elimination of batch effects.

Pyroptosis-related genes were obtained from the literature [11] and the Molecular Signatures Database (MSigDB), with a full list provided in Supplementary Table S1. Differentially expressed pyroptosis-related genes (DEGs) in the GSE93798 dataset were identified using the 'limma' package in R, with a significance threshold of $p < 0.05$ and $|\log_2 FC| \geq 0.5$. The expression profiles of these DEGs were visualized using the 'ggplot2' and 'pheatmap' packages to generate volcano plots and heatmaps, respectively. Overlapping genes were identified and illustrated with the 'VennDiagram' package. Protein–protein interactions (PPIs) were constructed with STRING v11.5/12 (organism: *Homo sapiens*, minimum interaction score 0.4) and visualized in Cytoscape (≥3.9).

2.2. Machine learning and identification of hub genes

To identify key genes associated with pyroptosis, two widely used machine learning algorithms – least absolute shrinkage and selection operator (LASSO) regression and support vector machine-recursive feature elimination (SVM-RFE) – were applied for feature selection. LASSO regression was implemented using the glmnet package in R, with 10-fold cross-validation to determine the optimal λ value that minimized the cross-validated mean squared error. The SVM-RFE model was constructed using the e1071 package with a radial basis function (RBF) kernel; the hyperparameters (C, γ) were optimized through grid search combined with fivefold cross-validation. Genes consistently selected by both algorithms were defined as hub genes. These overlapping genes demonstrated robust and consistent predictive value and were considered potential biomarkers for IgAN.

For classification modeling, GSE93798 served as the training set and GSE99339 as the external validation set. The training dataset (GSE93798) included 20 IgAN patients and 22 healthy controls, and the validation dataset (GSE99339) included 39 IgAN patients and 19 controls. Features comprised hub genes (with optional expansion to DEG subsets) after centering/scaling and pruning highly collinear variables ($|r| > 0.95$). We trained L2-regularized logistic regression, linear SVM, random forest, XGBoost, and Gaussian Naive Bayes within nested 5×5 cross-validation (inner folds for tuning, outer folds for performance). Models were combined via stacking (level-0 base learners; logistic regression meta-learner using

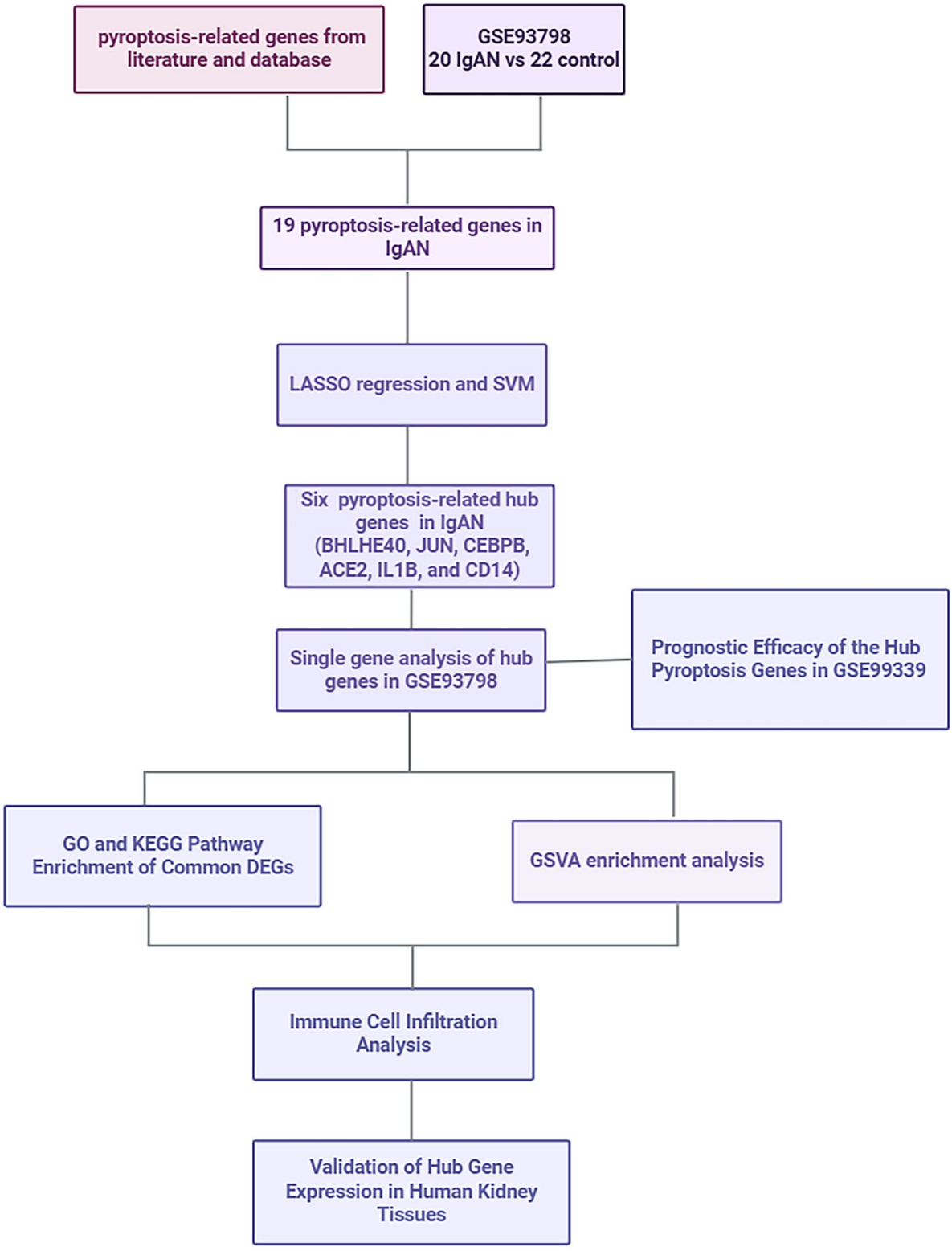

Figure 1. Schema of the study. Pyroptosis-related genes were collected from the literature and public databases and integrated with the GEO IgA nephropathy dataset GSE93798 (20 IgAN vs. 22 controls) to identify pyroptosis-related differentially expressed genes. Feature selection was performed using LASSO regression and support vector machine (SVM) algorithms, yielding six hub genes (BHLHE40, JUN, CEBPB, ACE2, IL1B, and CD14). Subsequent analyses included single-gene analysis, GO and KEGG pathway enrichment of common DEGs, GSVA enrichment analysis, immune cell infiltration analysis, and external validation in GSE99339, followed by experimental validation of hub gene expression in human kidney tissues and serum samples.

out-of-fold predictions) or, alternatively, soft-voting. Probabilities were calibrated by Platt scaling (SVM) or isotonic regression (others); stratified folds preserved class balance, and LASSO/mRMR feature selection was performed within each training fold to avoid leakage. The primary endpoint was ROC-AUC (with PR-AUC, accuracy, sensitivity, specificity, and Brier score as secondary metrics); thresholds were fixed by Youden's *J* on the training set and applied unchanged to validation. DeLong's test compared AUCs, and decision curve analysis was used where applicable. Model interpretability was assessed with SHAP, and reproducibility was ensured by fixed seeds (seed = 42) and fully encapsulated Scikit-learn pipelines.

2.3. Single gene analysis and enrichment analysis

Based on the identified core genes, samples were divided into high-expression and low-expression groups using *t*-tests. The clusterProfiler R package was employed to perform Gene Ontology (GO) and KEGG pathway enrichment analyses to explore the roles of these genes in important biological processes (BPs) such as immune response and cell migration. Additionally, GSEA (gene set enrichment analysis) was conducted using the GSEA software to analyze the expression differences of the target genes in various functions or pathways, further elucidating their biological functions and clinical significance.

2.4. Immune cell infiltration analysis

Immune-infiltration analysis was performed using the R package IOBR, employing the CIBERSORT, QUANTISEQ, and ESTIMATE algorithms to analyze the immune cell infiltration related to the core genes and investigate the changes in immune cell types and their potential roles in IgAN. CIBERSORT is a deconvolution algorithm that calculates the proportion of 22 immune cell types in each sample and the *p* value of the deconvolution result for each sample. Samples with a *p* value less than 0.01 were considered plausible.

2.5. Immunofluorescence and laboratory tests

Immunofluorescence staining for BHLHE40, c-JUN, CEBPB, ACE2, IL1B, and CD14 was performed for five IgAN patients and five paraneoplastic kidney tissues. Positive and negative controls were used to validate the antibody. After blocking, frozen tissue was incubated with the following antibodies: (1) BHLHE40 antibody (sc-101023, Santa Cruz Biotechnology, Dallas, TX) diluted 1:100, (2) c-JUN antibody (sc-166540, Santa Cruz Biotechnology, Dallas, TX) diluted 1:100, (3) CEBPB antibody (AF6202, Affinity, Cincinnati, OH) diluted 1:100, (4) ACE2 antibody (sc-390851, Santa Cruz Biotechnology, Dallas, TX) diluted 1:100, (5) IL1B antibody (26048-1-AP, Proteintech, Rosemont, IL) diluted 1:100, and (6) CD14 antibody (sc-1182, Santa Cruz Biotechnology, Dallas, TX) diluted 1:100 were incubated overnight at 4 °C. Then, it was washed with phosphate-buffered saline (PBS) obtained from Thermo Fisher Scientific (Waltham, MA), and then incubated at 4 °C for 1 h. Then, it was washed with PBS and incubated with Cy3-conjugated goat anti-mouse IgG (H + L) (SA00009-1, Proteintech, Rosemont, IL, 1:250) and fluorescein-conjugated goat anti-rabbit IgG (H + L) (SA00003-2, Proteintech, Rosemont, IL, 1:250). Sections were observed under a fluorescence microscope (Nikon, Tokyo, Japan) at a magnification of 400 using a Moticam 2506 instrument (Motic, Xiamen, China), and images were taken with a digital camera system (Nikon, Tokyo, Japan) for assessment in a blinded manner. Blinding was performed by having independent pathologists, who were not involved in the study, assess the slides without knowledge of the sample identities. Semi-quantitative assessments were performed using Image Pro-plus computer image analysis software (Media Cybernetics, Bethesda, MD) to analyze the fluorescence intensity and quantify protein levels. Five glomeruli from each biopsy tissue were randomly captured and analyzed, using the fluorescence intensity as the final result for each patient.

The study included 27 patients diagnosed with IgAN based on kidney biopsy results from 1 June 2021 to 31 December 2021. Laboratory tests were conducted to measure serum IgA concentration and serum IL-1 concentration. All laboratory tests were performed by the Department of Laboratory Medicine at the China-Japan Friendship Hospital. Written consent to publish these details has been obtained from all individuals (or their legal guardian).

2.6. Cell culture and treatment

Human mesangial cells (HMCs) were cultured in RPMI-1640 medium supplemented with 10% fetal bovine serum and 1% penicillin–streptomycin at 37 °C in a humidified 5% CO_2 atmosphere. Cells were divided into three groups: control, IgAN serum-treated, and LPS + ATP-stimulated. For the IgAN group, cells were incubated with 10% serum obtained from biopsy-confirmed IgAN patients for 24 h. The positive control group received 1 μg/mL LPS for 4 h followed by 5 mM ATP for 1 h to induce pyroptosis.

2.7. Western blot analysis

After treatment, total proteins were extracted using RIPA lysis buffer and quantified by the BCA method. Equal amounts of protein were separated by SDS-PAGE and transferred onto PVDF membranes. After blocking, membranes were incubated overnight at 4 °C with primary antibodies against c-JUN antibody (sc-166540, Santa Cruz Biotechnology, Dallas, TX) diluted 1:1,000, CEBPB antibody (AF6202, Affinity, Cincinnati, OH) diluted 1:1,000, ACE2 antibody (sc-390851, Santa Cruz Biotechnology, Dallas, TX) diluted 1:1,000, IL1B antibody (26048-1-AP, Proteintech, Rosemont, IL) diluted 1:1,000, CD14 antibody (sc-1182, Santa Cruz Biotechnology, Dallas, TX) diluted 1:1,000, followed by HRP-conjugated secondary antibodies. β-actin served as the loading control. Bands were visualized using enhanced chemiluminescence and analyzed by ImageJ (Bethesda, MD).

2.8. Statistical analysis

All analyses and graphs were performed under SPSS 26.0 (Chicago, IL) and R software (Version 4.1.2) (R Foundation for Statistical Computing, Vienna, Austria). Ggbeeswarm, ggpubr, and ggplot2 packages were used to plot box plots, and the significance of differences in continuous variables between the two groups was assessed by Student's *t*-test for normally distributed variables and Mann–Whitney's *U*-test for non-normally distributed variables. The pROC package was used to plot the ROC curve and AUC values were calculated. Spearman's coefficient was used to assess the correlation between continuous variables. Median survival differences were assessed by log-rank test. $p < 0.05$ was considered significant. In Western blot, data were expressed as mean ± SD. Comparisons among groups were performed using one-way ANOVA followed by Tukey's post hoc test. Correlations were assessed using Spearman's rank correlation. Statistical significance was set at $p < 0.05$.

3. Results

3.1. Identification of DEGs

After normalization, the mean gene expression values were uniformly consistent across all samples. Principal component analysis was used to assess between-group differences, confirming the plausibility of the sample data. A comprehensive examination of the IgAN dataset GSE93798 revealed 470 up-regulated and 598 down-regulated DEGs. The expression profile of the IgAN dataset was visualized, with the top 50 genes at both high and low expression levels depicted in a heatmap (Figure 2(A)) and a volcano plot (Figure 2(B)). The PCA plot (Figure 2(C)) demonstrates clear separation between the two groups, indicating distinct gene expression profiles.

We obtained 247 pyroptosis-related genes from the literature. Subsequently, we explored the expression of pyroptosis-related genes in IgAN and normal kidney tissues using the GSE93798 dataset. A total of 19 pyroptosis-related genes exhibited differential expression in IgAN (Figure 2(D)), with nine genes (IL1B, CD14, PGF, CLEC5A, PYCARD, GBP1, GZMA, BTK, and TLR2) up-regulated and 10 genes (BIRC3, BHLHE40, EPHA2, ACE2, DPEP1, JUN, CEBPB, PRDM1, TET2, and CD274) down-regulated (Figure 2(E,F)).

The PPI network constructed using the STRING database illustrates interactions among the 19 pyroptosis-related DEGs (Figure 2(G)). Network analysis identified IL1B, BTK, TLR2, JUN, CEBPB, and CD14 as hub genes with high connectivity, suggesting central roles in regulating pyroptosis and inflammation in IgAN. These genes are mainly involved in immune signaling, transcriptional regulation, and inflammatory responses, indicating their potential as key molecular targets in IgAN.

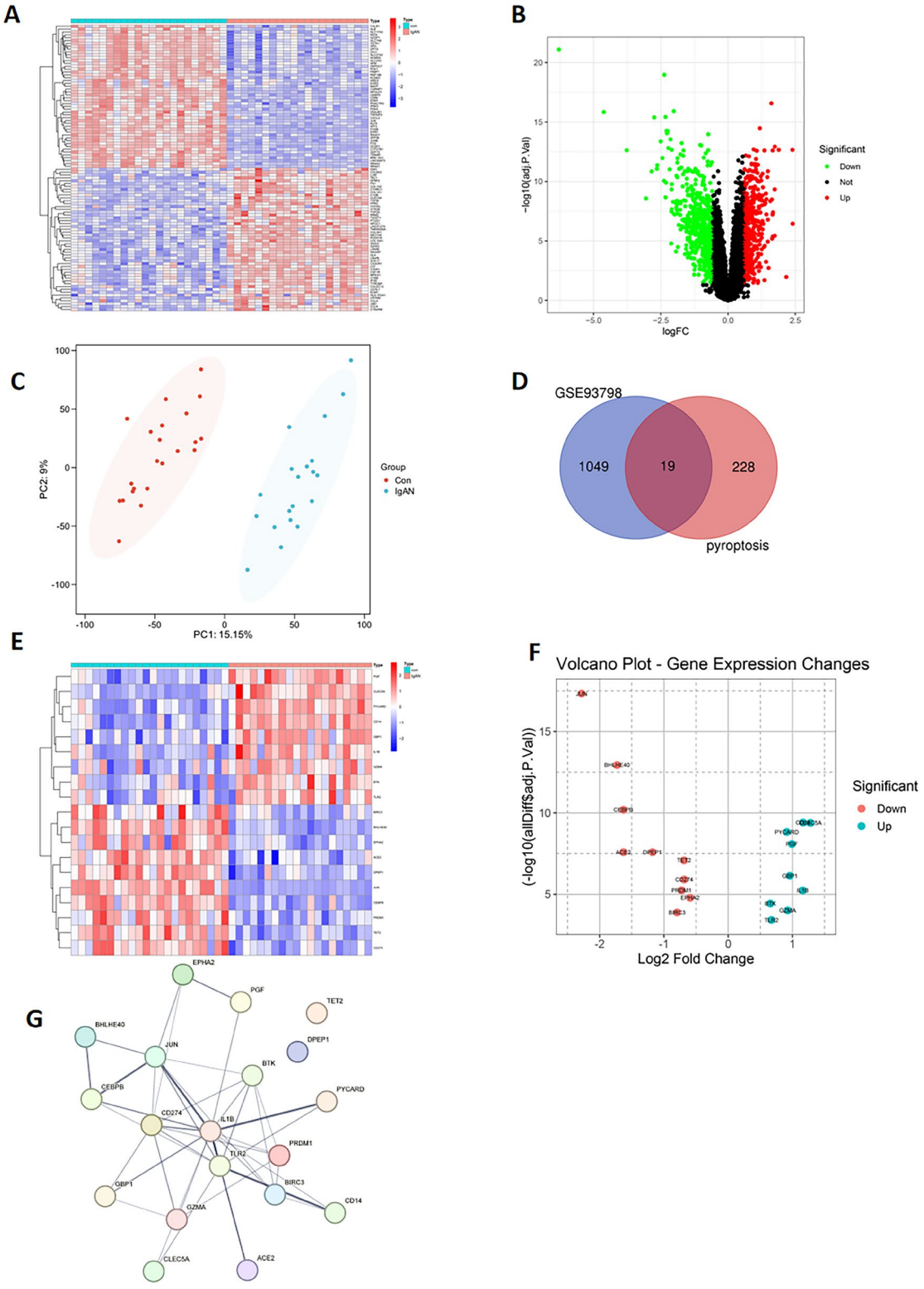

Figure 2. Differentially expressed gene identification. The heatmap (A) shows the top 50 upregulated and downregulated genes between the IgAN and control groups. The volcano plot (B) displays upregulated genes in light red and downregulated genes in light blue. The principal component analysis (PCA) plot (C) demonstrates clear separation between the two groups, indicating distinct gene expression profiles. The Venn diagram (D) illustrates the overlap between 1,068 DEGs from the GSE93798 dataset and pyroptosis-related genes. A total of 19 pyroptosis-related genes were differentially expressed in IgAN, including nine upregulated genes (IL1B, CD14, PGF, CLEC5A, PYCARD, GBP1, GZMA, BTK, and TLR2) and 10 downregulated genes (BIRC3, BHLHE40, EPHA2, ACE2, DPEP1, JUN, CEBPB, PRDM1, TET2, and CD274) (E). The volcano plot (F) further visualizes the expression changes of these pyroptosis-related genes. The protein–protein interaction (PPI) network (G) constructed from these 19 DEGs highlights key hub genes such as IL1B, BTK, TLR2, JUN, CEBPB, and CD14, suggesting their central role in IgAN-associated pyroptosis and inflammation.

3.2. Feature gene selection

Two machine learning algorithms were employed to identify IgAN-associated pyroptosis-related genes based on the differential analysis of the 19 genes. The LASSO algorithm, converging on the optimal lambda value, identified 11 key genes: BHLHE40, JUN, CEBPB, ACE2, IL1B, CD14, PGF, PYCARD, DPEP1, TET2, and BTK (Figure 3(A,B)). The SVM algorithm, based on the minimum discrimination error rate, identified seven key genes: BHLHE40, JUN, CEBPB, ACE2, IL1B, CD14, and CLEC5A (Figure 3(C,D)). Six genes (BHLHE40, JUN, CEBPB, ACE2, IL1B, and CD14) were considered by both algorithms to be the hub genes of pyroptosis in IgAN (Figure 3(E)).

3.3. Single gene analysis

Violin plots were used in the GSE93798 dataset to display the up-regulated and down-regulated expression trends of the six hub genes (IL1B, CD14, ACE2, JUN, CEBPB, and BHLHE40) and to determine whether the differences were statistically significant. The results showed that IL1B and CD14 were significantly up-regulated in the IgAN group (Figure 4(A,B)), while ACE2, JUN, CEBPB, and BHLHE40 were significantly down-regulated ($p < 0.05$) (Figure 4(C–F)). To explore the diagnostic efficacy of these hub genes, ROC analysis was performed in the GSE93798 dataset, revealing high diagnostic accuracy for discriminating IgAN from normal samples. The AUC values were as follows: IL1B (0.850), CD14 (0.964), ACE2 (0.952), JUN (1.000), BHLHE40 (0.991), and CEBPB (0.955).

3.4. Prognostic efficacy of the hub pyroptosis genes

The prognostic efficacy of the six hub genes was further validated in the GSE99339 dataset. The results showed that the differences in the expression of five genes (IL1B, CD14, ACE2, JUN, and BHLHE40) were consistent with those in the GSE93798 dataset ($p < 0.05$). ROC analysis in the GSE99339 dataset also demonstrated high diagnostic accuracy for discriminating IgAN from normal samples, with AUC values as follows: IL1B (0.900), CD14 (0.988), ACE2 (0.900), JUN (0.856), BHLHE40 (0.869), and CEBPB (0.900) (Figure 5).

A combined machine learning model integrating multiple algorithms (random forest, XGBoost, SVM, logistic regression, and Naive Bayes), shown in Figure 5(C), further improved diagnostic performance, achieving an AUC of 0.986 in the training set, suggesting strong predictive potential of the identified hub genes for IgAN diagnosis (Figure 5(C)).

To further validate the involvement of pyroptosis in IgAN, key executing genes (GSDMD, CASP1, CASP3, and NLRP3) were analyzed using the Nephroseq v5 database (Supplementary Figures S1 and S2). All four genes showed elevated expression in IgAN samples compared with controls, suggesting activation of the pyroptosis pathway in IgAN. Analysis of the Nephroseq v5 database revealed a close association between pyroptosis-related hub gene expression and clinical severity in IgAN. The expression levels of IL1B and CD14 were significantly higher in the high-proteinuria group compared with the low-proteinuria group ($p < 0.05$), indicating their potential involvement in immune activation and inflammation during disease progression. Similarly, JUN expression was markedly increased in the renal failure group relative to patients with normal renal function ($p < 0.05$), suggesting a role in the late-stage response of IgAN. These findings imply that dysregulation of pyroptosis-related genes correlates with clinical indicators of renal injury, supporting their potential utility as biomarkers for disease activity and progression.

3.5. GO and KEGG pathway enrichment of common DEGs

GO and KEGG pathway enrichment analyses were conducted on the 19 pyroptosis-related DEGs to explore the biological functions and pathways involved in IgAN pyroptosis. The top 10 terms in each category (BP, CC, and MF) were visualized in bubble plots (Figure 6(A,B)). The KEGG analyses are shown in Figure 6(C,D). The BP subset indicated that common DEGs are involved in the humoral immune response, defense response to bacterium, complement activation, leukocyte migration, synapse pruning,

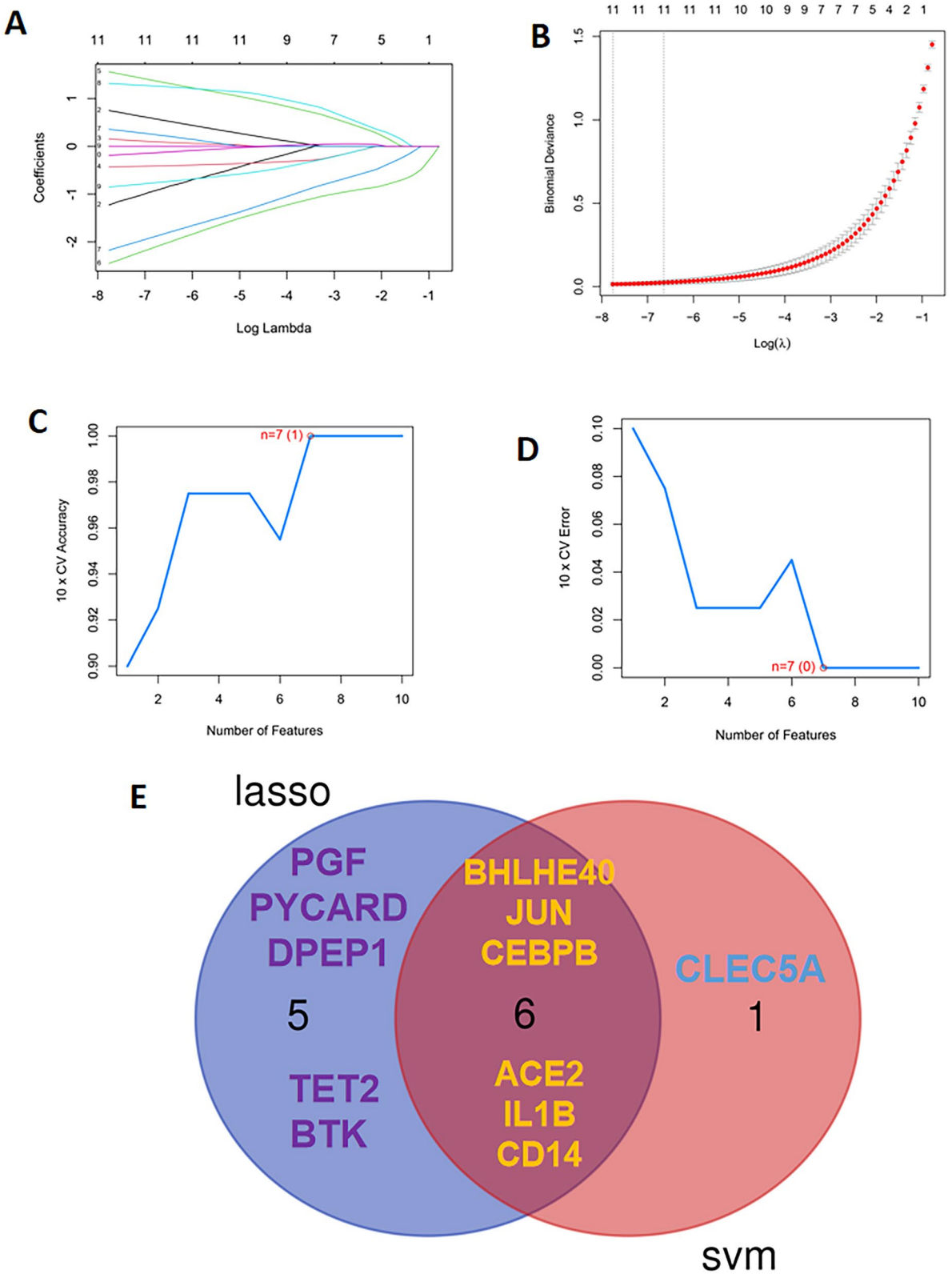

Figure 3. Identification of hub genes. The LASSO algorithm identified 11 significant genes (A, B). The SVM algorithm identified seven genes (C, D). The Venn diagram (E) shows the overlap of six hub genes of IgAN.

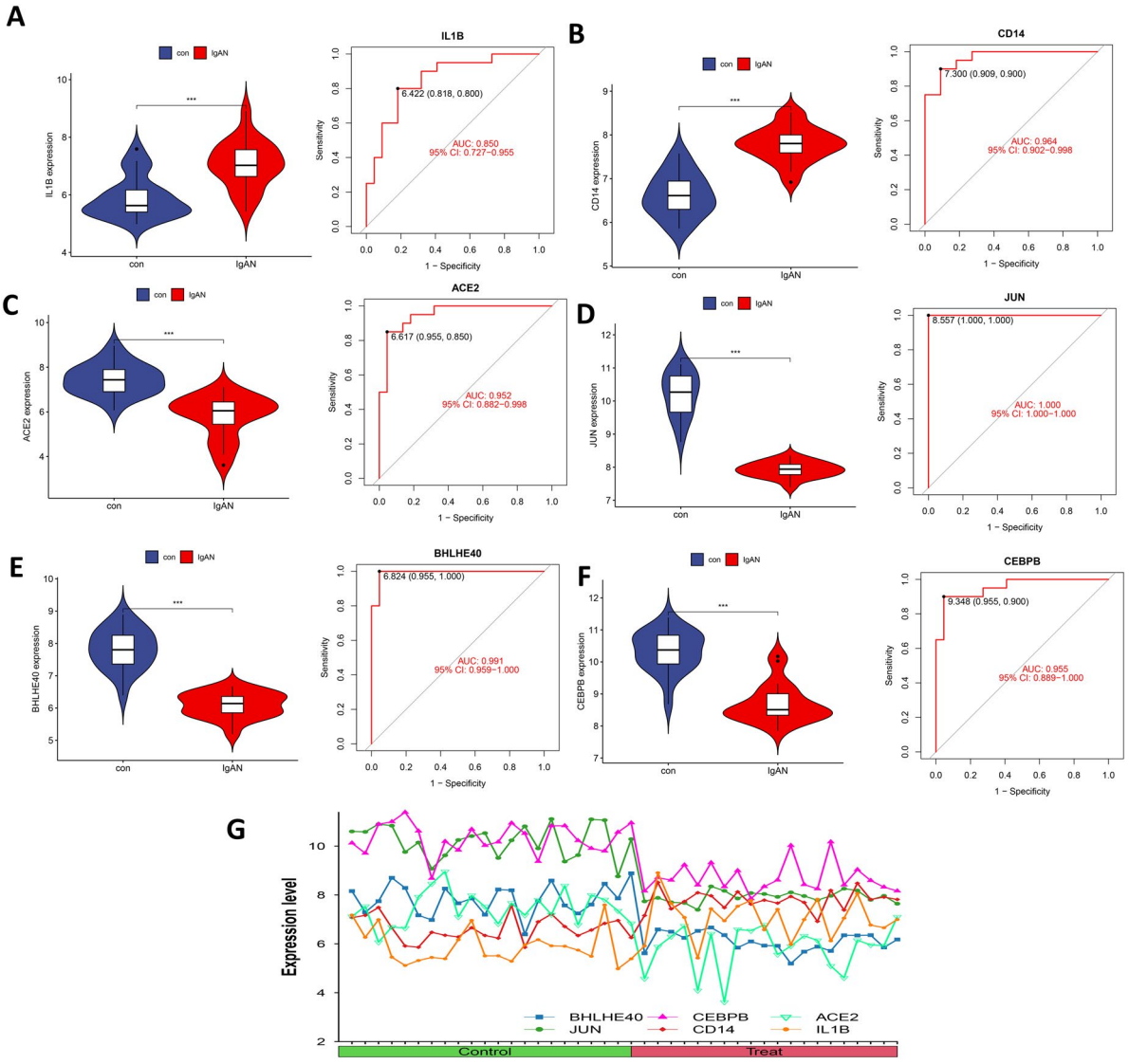

Figure 4. Single gene analysis. Violin plots in GSE93798 of the expression of six hub genes. IL1B and CD14 were significantly up-regulated in the IgAN group (A, B), while ACE2, JUN, CEBPB, and BHLHE40 were significantly down-regulated ($p < 0.05$) (C–F). ROC analysis revealed AUC values: IL1B (0.850), CD14 (0.964), ACE2 (0.952), JUN (1.000), BHLHE40 (0.991), and CEBPB (0.955). (E) A line graph of gene expression of the six hub genes in the control and IgAN groups.

activation of immune response, response to molecule of bacterial origin, and myeloid leukocyte activation. The cellular component (CC) subset highlighted involvement in the collagen-containing extracellular matrix, secretory granule lumen, and cytoplasmic vesicle lumen. Molecular function (MF) elucidated roles in peptidase regulator activity, enzyme inhibitor activity, and endopeptidase inhibitor activity. KEGG pathway enrichment analysis underscored the significant participation of the common DEGs in complement and coagulation cascades, PI3K-Akt signaling pathway, pertussis, *Staphylococcus aureus* infection, legionellosis, and alcoholic liver disease.

Figure 6 shows the top 10 significantly enriched terms in the BP, MF, and CC categories, which reveal that these DEGs are enriched in BP, including complement activation, humoral immune response and circulating immunoglobulin-mediated humoral immune response, as well as in CC, which includes immunoglobulin complexes, outer plasma membrane, and collagen-containing extracellular matrix, and in MF, which includes antigen-binding, immunoglobulin receptor-binding, and extracellular matrix structural components. MF includes antigen binding, immunoglobulin receptor binding, and structural components of the extracellular matrix. Enrichment of the KEGG pathway yielded 30 related pathways. These pathways were enriched for extracellular structure composition, immune cell activation, immunoglobulin-mediated

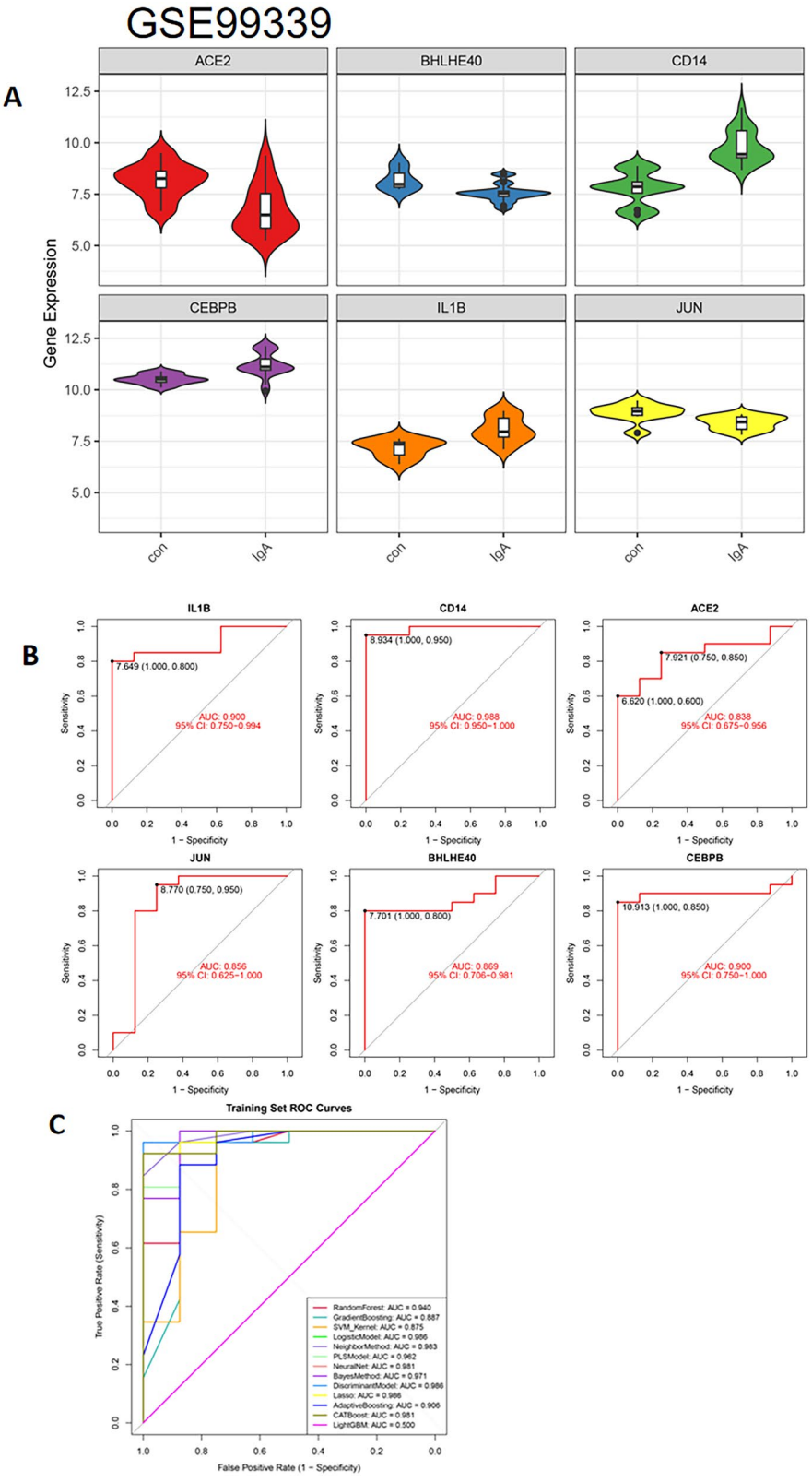

Figure 5. Validation of hub genes in the GSE99339 Dataset. The validation results in the GSE99339 dataset were consistent with those in the GSE93798 dataset for five genes: IL1B, CD14, ACE2, JUN, and BHLHE40 ($p < 0.05$). ROC analysis demonstrated high diagnostic accuracy for discriminating IgAN from normal samples, with AUC values of IL1B (0.900), CD14 (0.988), ACE2 (0.900), JUN (0.856), BHLHE40 (0.869), and CEBPB (0.900). (C) A combined machine learning model integrating multiple algorithms (random forest, XGBoost, SVM, logistic regression, and Naive Bayes) further improved diagnostic performance, achieving an AUC of 0.986 in the training set, suggesting strong predictive potential of the identified hub genes for IgAN diagnosis.

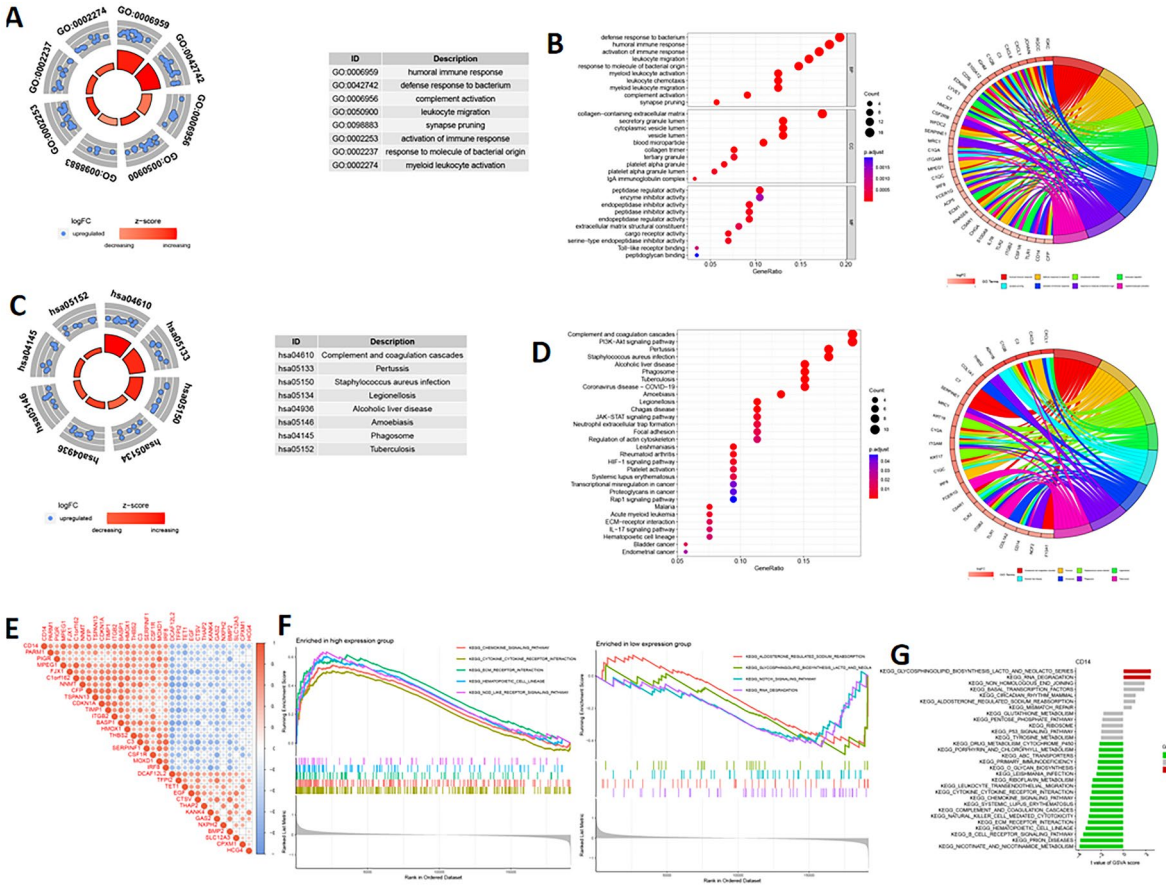

Figure 6. Results of GO, KEGG, and GSVA pathway enrichment analysis. GO and KEGG pathway enrichment analyses were performed on the identified differentially expressed genes (DEGs). Adjusted $p < 0.05$ was considered significant. (A, B) The top 10 significantly enriched terms in biological process (BP), molecular function (MF), and cellular component (CC) categories are shown in bubble plots. (C, D) KEGG pathway enrichment analysis identified 30 related pathways. (E–G) GSVA enrichment analysis showed the pathways enriched in high-expression and low-expression groups.

immune responses, humoral immune responses, immunoglobulin complex cytokine receptor interactions, and autoimmune diseases (systemic lupus erythematosus), as shown in Figure 6(D).

3.6. GSVA analysis

In order to explore the differences in BPs among the different pattern clusters mediated by pyroptosis, we performed GSVA enrichment analysis and found that the high expression group was mainly enriched in cytokine interactions and extracellular matrix-associated pathways (KEGG_CHEMOKINE_SIGNALING_PATHWAY, KEGG_CYTOKINE_CYTOKINE_RECEPTOR_INTERTERRACER, KEGG_CYTOKINE_CYTOKINE_CYTOKINE_CYTOKINE_CYTOKINE_RECEPTOR_INTERRACER, RECEPTOR_INTERACTION, KEGG_ECM_RECEPTOR_INTERACTION), whereas the low-expression group was enriched in aldosterone electrolyte reabsorption and NOTCH signaling pathways, as shown in Figure 6(E,F,G).

3.7. Immune cell infiltration analysis

The CIBERSORT algorithm, which stands for Cell-type Identification By Estimating Relative Subsets Of RNA Transcripts, was employed to calculate the infiltration levels of 22 immune cell types across various samples. These results were visualized in a stacked bar chart (Figure 7(A)). The Wilcoxon test was used to compare the differences in immune infiltration scores. IgAN samples were divided into two groups based on the high and low expression of the key gene CD14. The high-expression group exhibited higher levels of CD8+ T cells, cytolytic activity, macrophages, pDC (plasmacytoid dendritic cells), and TILs (tumor-infiltrating lymphocytes).

The immune infiltration abundance of 28 immune cell types in the normal and DN (disease-negative) groups was also represented in a stacked bar chart (Figure 7(B)). Additionally, the immune infiltration scores of IgAN samples and control samples were calculated, revealing significant differences in seven cell types. In the IgAN group, higher infiltration levels were observed for B cells, plasma cells, CD8 T cells, M2 macrophages, and neutrophils, while lower infiltration levels were seen for resting NK cells and neutrophils. The control group exhibited the opposite trend (Figure 7(C)).

3.8. Validation of hub gene expression in human kidney tissues

To further validate the results of the bioinformatics analysis, immunofluorescence staining and ELISA of serum IgA and serum IL-1 concentration were performed to assess the protein expression of IL1B, CD14, ACE2, JUN, CEBPB, and BHLHE40 in kidney tissue samples from IgAN patients and healthy individuals. Representative images of the immunofluorescence staining are shown in Figure 8. Compared to the control group, the IgAN group exhibited significantly up-regulated expression of IL-1β and CD14 (Figure 8(M)). The Spearman correlation analysis indicates a significantly positive correlation between serum IL-1 concentration and serum IgA (r = 0.41, p = 0.003). Statistical significance was set at $p < 0.05$.

In vitro, HMCs treated with IgAN patient serum displayed morphological and molecular features consistent with pyroptosis, similar to those induced by LPS + ATP stimulation. Western blot analysis (Figure 8(O,P)) showed elevated expression of CD14, IL1B, and Pro-IL1B, accompanied by reduced ACE2 and JUN levels. CEBPB showed no significant change. These results indicate that exposure to IgAN serum can trigger

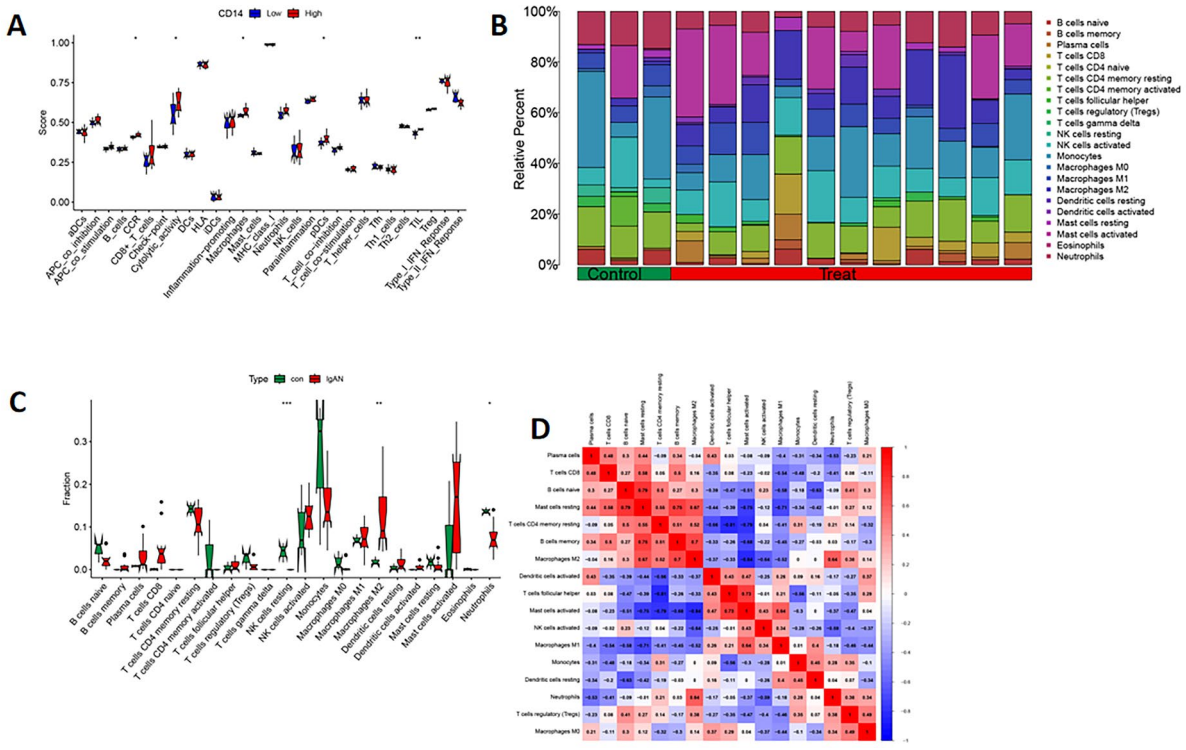

Figure 7. Immune cell enrichment and correlation analysis in IgAN. (A) Differences in the enrichment abundance of 22 immune cells between the normal and DN groups in the combined dataset, with the normal group in blue and the experimental group in pink. The *x*-axis represents the 22 immune cells, and the *y*-axis represents the immune cell infiltration abundance. IgAN samples were grouped based on high and low expression of the key gene CD14, and the immune infiltration scores were calculated for different groups. (B, C) Immune infiltration scores of IgAN and control samples to determine the relative proportions of 22 infiltrating immune cells, with significant differences found in seven cell types. (D) Subgroup correlation analysis of immune cells showed significant differences in infiltration abundance. The color indicates the strength of the correlation, with redder colors representing stronger correlations between two immune cells. The symbols are as follows: $^{ns}p > 0.05$ (not statistically significant); $^{*}p < 0.05$ (statistically significant); $^{**}p < 0.01$ (highly significant); $^{***}p < 0.001$ (extremely significant).

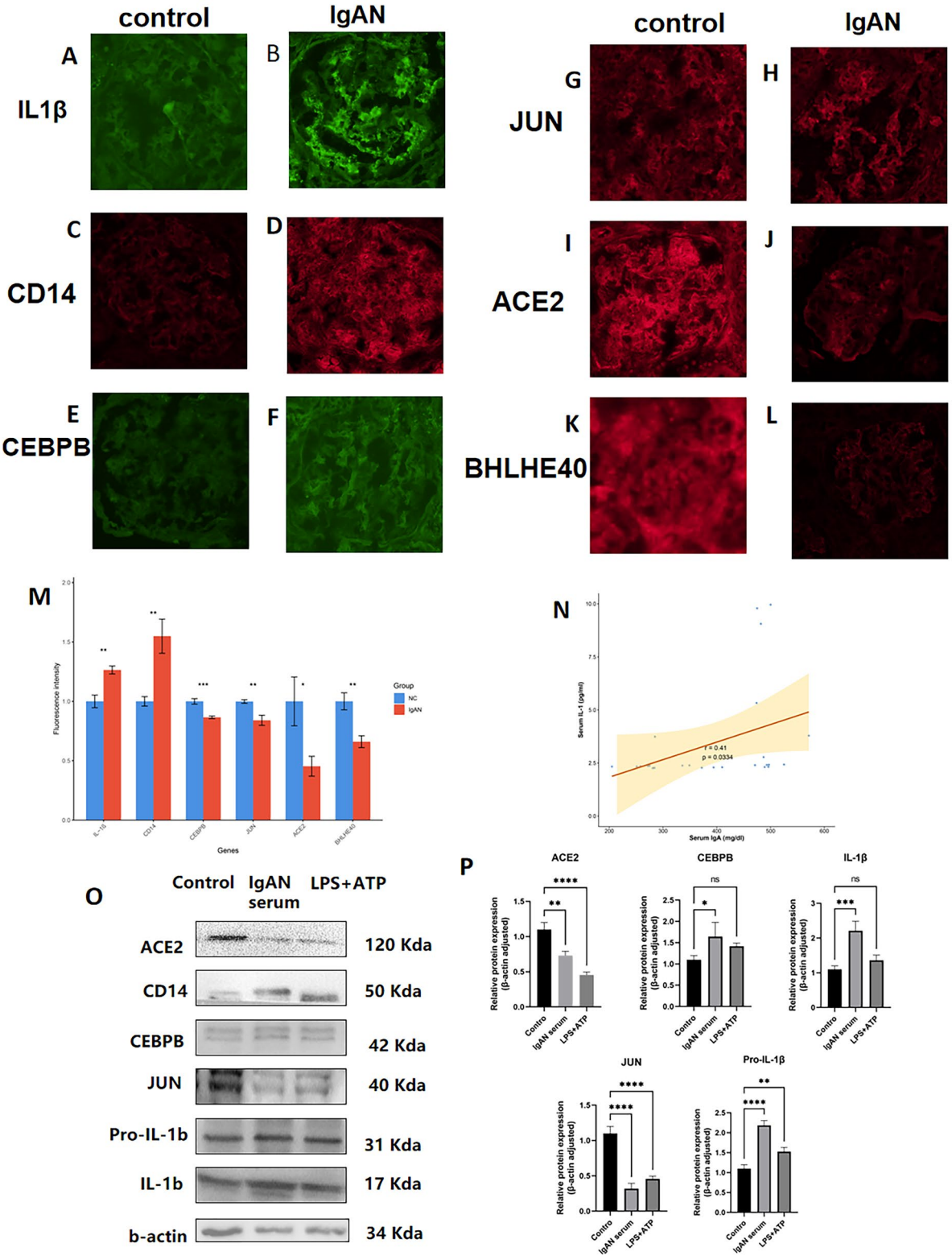

Figure 8. Immunofluorescence staining for key genes in IgAN kidney samples. (A–L) Representative images of immunofluorescence staining for IL1B, CD14, ACE2, JUN, CEBPB, and BHLHE40 in IgAN and control kidney samples ($N = 3$ to 3). (M) Statistical analysis of immunohistochemical staining. Data are presented as mean ± mean squared error (MSE). (N) The Spearman's correlation analysis indicates a positive correlation between serum IL-1 concentration and serum IgA ($r = 0.41$, $p = 0.003$). (O) Western blot (WB) analysis of ACE2, CD14, CEBPB, JUN, and IL1B in control, IgAN serum-treated, and LPS + ATP-stimulated mesangial cells. (P) Quantification of WB band intensity revealed significant upregulation of CD14, IL1B, and Pro-IL1B, and downregulation of ACE2 and JUN in IgAN and LPS + ATP groups compared with controls. Data are shown as mean ± SD, with *$p < 0.05$, **$p < 0.01$, ***$p < 0.001$, and ****$p < 0.0001$.

pyroptotic activation in mesangial cells, paralleling the effects of classical inflammasome activation by LPS + ATP, thus confirming the inflammatory cell death pathway involvement in IgAN pathogenesis.

4. Discussion

Our study identified 19 pyroptosis-related differentially expressed genes (DEGs) in IgAN, including nine up-regulated genes (IL1B, CD14, PGF, CLEC5A, PYCARD, GBP1, GZMA, BTK, and TLR2) and 10 down-regulated genes (BIRC3, BHLHE40, EPHA2, ACE2, DPEP1, JUN, CEBPB, PRDM1, TET2, and CD274). Machine learning algorithms further identified six hub genes (BHLHE40, JUN, CEBPB, ACE2, IL1B, and CD14) with high diagnostic accuracy for discriminating IgAN from normal samples, suggesting their potential as biomarkers for IgAN. GO and KEGG enrichment analyses revealed that these DEGs are involved in immune response, cell migration, and inflammation pathways, consistent with the known role of inflammation in IgAN pathogenesis and the potential involvement of pyroptosis in disease progression. Immune cell infiltration analysis showed significantly higher levels of CD8+ T cells, macrophages, and neutrophils in IgAN compared to controls, highlighting the critical role of immune cell infiltration in IgAN pathogenesis and providing potential therapeutic targets for the disease.

In this study, IL-1β emerged as a key pyroptosis-associated gene in IgAN. Pyroptosis is an inflammatory mode of programmed cell death that acts as a defense mechanism against microbial invasion. This process can proceed via canonical and non-canonical pathways [12–14]. While the canonical pathway is activated by pathogen- and damage-associated molecular patterns (PAMPs and DAMPs), the non-canonical pathway specifically recognizes intracellular lipopolysaccharides (LPS) from Gram-negative bacteria. In both routes, the terminal step involves cleavage of GSDMD by caspase-1 (canonical) or caspases-4/5/11 (non-canonical) [15–17]. The cleaved GSDMD-N fragment forms membrane pores, facilitating the release of pro-inflammatory mediators like IL-1β and IL-18, disrupting ionic equilibrium, and ultimately inducing cell rupture and inflammation [18–21].

Our findings show elevated IL-1β expression in IgAN, corroborating previous studies. IL-1β and its receptor share downstream signaling cascades with Toll-like receptors (TLRs), contributing to cytokine production. IL-1 receptor antagonist (IL-1Ra) counteracts these effects, and the IL-1Ra/IL-1β ratio is considered a marker of immune balance. Notably, a lower ratio has been linked to more aggressive renal pathology in IgAN [22]. Additionally, a polymorphism in IL-1B (rs1143627) has been implicated in increased susceptibility to IgAN among the Chinese Han population [23].

Another gene of interest, CD14, was also upregulated and highlighted as a pyroptosis-related hub. CD14 functions as a co-receptor on macrophages, facilitating the recognition of LPS and oxidized lipids. Initially identified for its role in LPS-mediated cytokine release during sepsis, CD14 is now known to also modulate metabolic activity under innate immune activation [24,25]. Genetic variants in CD14 have been associated with IgAN progression, arterial stiffness [26,27], and hypertension [28,29].

Our immune infiltration analysis revealed increased M2 macrophage infiltration in the glomeruli of IgAN patients. Previous reports have demonstrated similar findings, including enrichment of M2 macrophage subsets (e.g., $CD163^+$, $CD206^+$, and $CD86^+$), each contributing uniquely to disease development [30]. Certain subtypes, such as M2b and M2c, have shown strong correlations with crescent formation, eGFR decline, and proteinuria, indicating their involvement in acute kidney injury (AKI) associated with IgAN [31].

The primary pathological event in IgAN involves deposition of galactose-deficient IgA1, immune complexes, and complement components [32,33]. These deposits activate resident mesangial cells and infiltrating macrophages via complement receptors, Fc receptors, or MHC-II molecules [34]. This activation contributes to mesangial expansion, segmental lesions, and endocapillary hypercellularity. Early infiltration by macrophages appears to influence phenotypic transformation of mesangial cells, potentially driving glomerular sclerosis. This transformation is associated with α-SMA expression, a key marker of fibrosis, which has also been shown to predict renal function deterioration in IgAN [34,35].

Moreover, three downregulated genes – c-JUN, ACE2, and BHLHE40 (DEC1) – were identified as pyroptosis-related markers in IgAN. JUN, a component of the AP-1 transcription factor complex, is involved in proliferation and stress signaling. Its expression was significantly reduced in regulatory T cells from patients with IgAN complicated by nephrotic syndrome [35].

ACE2, known for its renoprotective, anti-inflammatory, and anti-fibrotic properties, was found to be downregulated. This reduction may impair the kidney's ability to counteract fibrogenic and inflammatory insults, potentially exacerbating IgAN progression [36]. An imbalance between ACE and ACE2 has been implicated in disease development, and recombinant ACE2 has demonstrated protective effects in experimental models of Alport syndrome.

DEC1 (BHLHE40), a bHLH transcription factor, regulates immune activity, circadian rhythm, and cellular metabolism. While direct evidence linking DEC1 to IgAN remains scarce, its established role in T cell function and inflammation suggests it may influence IgAN pathophysiology indirectly. Similarly, CEBPB, a transcription factor involved in inflammatory signaling, has been shown to be upregulated in other kidney diseases such as lupus nephritis. Though its role in IgAN has not been extensively explored, its regulatory influence on immune pathways indicates it could contribute to the disease's inflammatory landscape.

Our study identified 19 pyroptosis-related DEGs in IgAN, including nine up-regulated genes (IL1B, CD14, PGF, CLEC5A, PYCARD, GBP1, GZMA, BTK, and TLR2) and 10 down-regulated genes (BIRC3, BHLHE40, EPHA2, ACE2, DPEP1, JUN, CEBPB, PRDM1, TET2, and CD274). Machine learning algorithms further identified six hub genes (BHLHE40, JUN, CEBPB, ACE2, IL1B, and CD14) with high diagnostic accuracy for discriminating IgAN from normal samples, suggesting their potential as biomarkers for IgAN. GO and KEGG enrichment analyses revealed that these DEGs are involved in immune response, cell migration, and inflammation pathways, consistent with the known role of inflammation in IgAN pathogenesis and the potential involvement of pyroptosis in disease progression. Immune cell infiltration analysis showed significantly higher levels of CD8+ T cells, macrophages, and neutrophils in IgAN compared to controls, highlighting the critical role of immune cell infiltration in IgAN pathogenesis and providing potential therapeutic targets for the disease.

Our findings suggest a potential IL1B–CD14–TLR2–BTK signaling axis involved in inflammation and pyroptosis in IgAN. Upstream CD14/TLR2 may activate the MyD88–NF-κB pathway to promote IL1B expression, consistent with previous single-cell studies showing innate immune activation in IgAN kidneys [37]. BTK has been reported to regulate the NLRP3 inflammasome, leading to caspase-1-mediated GSDMD cleavage and IL-1β release [38,39]. In our WB results, IL1B, CD14, and JUN were upregulated, while ACE2 decreased in IgAN serum-treated mesangial cells, similar to LPS + ATP stimulation. Since ACE2 exerts anti-inflammatory and renoprotective effects, its reduction may enhance pyroptotic signaling [40,41]. Although this axis has not been experimentally confirmed, our data imply its possible involvement in IgAN pathogenesis and suggest ACE2 or IL1B as potential therapeutic targets.

This study has a few limitations. First, we did not have access to detailed clinical data from the patients, including factors like age, gender, and disease duration, which could influence gene expression. Additionally, a larger cohort of IgAN patients is needed to confirm the robustness of our findings. Furthermore, although the perfect AUC value of JUN (1.0) suggests a possibility of overfitting, its consistent differential expression and strong discriminative performance support JUN as a biologically plausible hub gene that warrants validation in larger, clinically annotated cohorts.

Acknowledgments

Jiayi Li: conceptualization, methodology, software, formal analysis, investigation, data curation, writing – original draft, writing – review and editing, project administration. Cheng Zhou: methodology, investigation, data curation. Shunlai Shang: methodology, data curation, validation. Qianqian Xu: methodology, data curation, formal analysis, writing – original draft. Wenge Li: conceptualization, resources, supervision, project administration. All authors contributed to the work reported in the manuscript and approved the final version. Any deviations or external contributions are clearly indicated within the text.

Author contributions

CRediT: **Jiayi Li**: Conceptualization, Data curation, Project administration, Validation, Visualization, Writing – original draft; **Cheng Zhou**: Conceptualization, Formal analysis, Supervision, Writing – review & editing; **Shunlai Shang**: Conceptualization, Writing – review & editing; **Qianqian Xu**: Conceptualization, Funding acquisition, Writing – review & editing; **Wenge Li**: Conceptualization, Funding acquisition, Writing – review & editing.

Disclosure statement

No potential conflict of interest was reported by the author(s).

Ethical approval

This study was conducted in accordance with the guidelines of the Declaration of Helsinki and was approved by the Ethics Committee of China-Japan Friendship Hospital (approval number: 2019-17-K12).

Consent form

Written consent to publish these details has been obtained from all individuals (or their legal guardian).

Funding

This work was supported by grant from National High Level Hospital Clinical Research Funding (2025-NHLHCRF-JBGS -A-WZ-05).

Data availability statement

The data that support the findings of this study are available from the corresponding author, Wenge Li, upon reasonable request.

References

[1] Donadio JV, Grande JP. IgA nephropathy. N Engl J Med. 2002;347(10):738–748. doi:10.1056/NEJMra020109.
[2] Lai KN, Tang SCW, Schena FP, et al. IgA nephropathy. Nat Rev Dis Primers. 2016;2(1):16001. doi:10.1038/nrdp.2016.1.
[3] Coppo R. Treatment of IgA nephropathy: recent advances and prospects. Nephrol Ther. 2018;14(Suppl. 1):S13–S21. doi:10.1016/j.nephro.2018.02.010.
[4] Lai KN. Pathogenesis of IgA nephropathy. Nat Rev Nephrol. 2012;8(5):275–283. doi:10.1038/nrneph.2012.58.
[5] Rajasekaran A, Julian BA, Rizk DV. IgA nephropathy: an interesting autoimmune kidney disease. Am J Med Sci. 2021;361(2):176–194. doi:10.1016/j.amjms.2020.10.003.
[6] El Karoui K, Fervenza FC, De Vriese AS. Treatment of IgA nephropathy: a rapidly evolving field. J Am Soc Nephrol. 2024;35(1):103–116. doi:10.1681/ASN.0000000000000242.
[7] Peng W, Pei GQ, Tang Y, et al. IgA1 deposition may induce NLRP3 expression and macrophage transdifferentiation of podocyte in IgA nephropathy. J Transl Med. 2019;17(1):406. doi:10.1186/s12967-019-02157-2.
[8] Wu C-Y, Hua K-F, Yang S-R, et al. Tris DBA ameliorates IgA nephropathy by blunting the activating signal of NLRP3 inflammasome through SIRT1- and SIRT3-mediated autophagy induction. J Cell Mol Med. 2020;24(23):13609–13622. doi:10.1111/jcmm.15663.
[9] Zhang L, Wang XZ, Li YS, et al. Icariin ameliorates IgA nephropathy by inhibition of nuclear factor kappa b/Nlrp3 pathway. FEBS Open Bio. 2017;7(1):54–63. doi:10.1002/2211-5463.12161.
[10] Danelishvili L, Everman JL, McNamara MJ, et al. Inhibition of the plasma-membrane-associated serine protease cathepsin G by *Mycobacterium tuberculosis* Rv3364c suppresses caspase-1 and pyroptosis in macrophages. Front Microbiol. 2011;2:281. doi:10.3389/fmicb.2011.00281.
[11] Ye Y, Dai Q, Qi H. A novel defined pyroptosis-related gene signature for predicting the prognosis of ovarian cancer. Cell Death Discov. 2021;7(1):71. doi:10.1038/s41420-021-00451-x.
[12] He W-T, Wan H, Hu L, et al. Gasdermin D is an executor of pyroptosis and required for interleukin-1β secretion. Cell Res. 2015;25(12):1285–1298. doi:10.1038/cr.2015.139.
[13] Kayagaki N, Stowe IB, Lee BL, et al. Caspase-11 cleaves gasdermin D for non-canonical inflammasome signalling. Nature. 2015;526(7575):666–671. doi:10.1038/nature15541.
[14] Song Q, Burrows SR, Smith G, et al. Interleukin-1 beta-converting enzyme-like protease cleaves DNA-dependent protein kinase in cytotoxic T cell killing. J Exp Med. 1996;184(2):619–626. doi:10.1084/jem.184.2.619.
[15] Sborgi L, Rühl S, Mulvihill E, et al. GSDMD membrane pore formation constitutes the mechanism of pyroptotic cell death. EMBO J. 2016;35(16):1766–1778. doi:10.15252/embj.201694696.
[16] de Vasconcelos NM, Van Opdenbosch N, Van Gorp H, et al. Single-cell analysis of pyroptosis dynamics reveals conserved GSDMD-mediated subcellular events that precede plasma membrane rupture. Cell Death Differ. 2019;26(1):146–161. doi:10.1038/s41418-018-0106-7.

[17] Rathinam VAK, Zhao Y, Shao F. Innate immunity to intracellular LPS. Nat Immunol. 2019;20(5):527–533. doi:10.1038/s41590-019-0368-3.
[18] Szekanecz Z, Szamosi S, Kovács GE, et al. The NLRP3 inflammasome–interleukin 1 pathway as a therapeutic target in gout. Arch Biochem Biophys. 2019;670:82–93. doi:10.1016/j.abb.2019.01.031.
[19] Broz P, Dixit VM. Inflammasomes: mechanism of assembly, regulation and signalling. Nat Rev Immunol. 2016;16(7):407–420. doi:10.1038/nri.2016.58.
[20] Liu X, Zhang Z, Ruan J, et al. Inflammasome-activated gasdermin D causes pyroptosis by forming membrane pores. Nature. 2016;535(7610):153–158. doi:10.1038/nature18629.
[21] Chen Q, Shi P, Wang Y, et al. GSDMB promotes non-canonical pyroptosis by enhancing caspase-4 activity. J Mol Cell Biol. 2019;11(6):496–508. doi:10.1093/jmcb/mjy056.
[22] Rauta V, Teppo AM, Törnroth T, et al. Lower urinary-interleukin-1 receptor-antagonist excretion in IgA nephropathy than in Henoch–Schönlein nephritis. Nephrol Dial Transplant. 2003;18(9):1785–1791. doi:10.1093/ndt/gfg234.
[23] Ding X, Mei Y, Mao Z, et al. Association of immune and inflammatory gene polymorphism with the risk of IgA nephropathy: a systematic review and meta-analysis of 45 studies. Front Immunol. 2021;12:683913. doi:10.3389/fimmu.2021.683913.
[24] Furnkranz A, Schober A, Bochkov VN, et al. Oxidized phospholipids trigger atherogenic inflammation in murine arteries. Arterioscler Thromb Vasc Biol. 2005;25(3):633–638. doi:10.1161/01.ATV.0000153106.03644.a0.
[25] Pahwa R, Devaraj S, Jialal I. The effect of the accessory proteins, soluble CD14 and lipopolysaccharide-binding protein on Toll-like receptor 4 activity in human monocytes and adipocytes. Int J Obes. 2016;40(6):907–911. doi:10.1038/ijo.2016.32.
[26] Yoon H-J, Shin JH, Yang SH, et al. Association of the CD14 gene −159C polymorphism with progression of IgA nephropathy. J Med Genet. 2003;40(2):104–108. doi:10.1136/jmg.40.2.104.
[27] Kheradmand M, Niimura H, Kuwabara K, et al. Association of inflammatory gene polymorphisms and conventional risk factors with arterial stiffness by age. J Epidemiol. 2013;23(6):457–465. doi:10.2188/jea.je20130054.
[28] Wang W, Sun Y, Fu Y, et al. The effects of both single-locus and multi-locus interaction on the clinical manifestations of IgA nephropathy in Southern Han Chinese. Nephrol Dial Transplant. 2014;29(3):550–555. doi:10.1093/ndt/gft468.
[29] Fehrenbach DJ, Abais-Battad JM, Dasinger JH, et al. Sexual dimorphic role of CD14 (cluster of differentiation 14) in salt-sensitive hypertension and renal injury. Hypertension. 2021;77(1):228–240. doi:10.1161/hypertensionaha.120.14928.
[30] Yang M, Liu JW, Zhang YT, et al. The role of renal macrophage, AIM, and TGF-β1 expression in renal fibrosis progression in IgAN patients. Front Immunol. 2021;12:646650. doi:10.3389/fimmu.2021.646650.
[31] Li J, Yu Y-F, Liu C-H, et al. Significance of M2 macrophages in glomerulonephritis with crescents. Pathol Res Pract. 2017;213(9):1215–1220. doi:10.1016/j.prp.2017.04.011.
[32] Suzuki H. Biomarkers for IgA nephropathy on the basis of multi-hit pathogenesis. Clin Exp Nephrol. 2019;23(1):26–31. doi:10.1007/s10157-018-1582-2.
[33] Hiki Y, Odani H, Takahashi M, et al. Mass spectrometry proves under-O-glycosylation of glomerular IgA1 in IgA nephropathy. Kidney Int. 2001;59(3):1077–1085. doi:10.1046/j.1523-1755.2001.00591.x.
[34] Nagata M, Akioka Y, Tsunoda Y, et al. Macrophages in childhood IgA nephropathy. Kidney Int. 1995;48(2):527–535. doi:10.1038/ki.1995.323.
[35] Chen Q, Jiang H, Ding R, et al. Cell-type-specific molecular characterization of cells from circulation and kidney in IgA nephropathy with nephrotic syndrome. Front Immunol. 2023;14:1231937. doi:10.3389/fimmu.2023.1231937.
[36] Mizuiri S, Hemmi H, Arita M, et al. Increased ACE and decreased ACE2 expression in kidneys from patients with IgA nephropathy. Nephron Clin Pract. 2011;117(1):c57–c66. doi:10.1159/000319648.
[37] Liu F, Chen H, Cao C, et al. The role of toll-like receptors (TLRs) and their therapeutic applications in glomerulonephritis. Int Urol Nephrol. 2023;55(11):2845–2856. doi:10.1007/s11255-023-03592-3.
[38] Bittner ZA, Liu X, Mateo Tortola M, et al. BTK operates a phospho-tyrosine switch to regulate NLRP3 inflammasome activity. J Exp Med. 2021;218(11):e20201656. doi:10.1084/jem.20201656.
[39] Shi J, Zhao Y, Wang K, et al. Cleavage of GSDMD by inflammatory caspases determines pyroptotic cell death. Nature. 2015;526(7575):660–665. doi:10.1038/nature15514.
[40] Zheng J, Hao H. Targeting renal damage: the ACE2/Ang-(1–7)/mas axis in chronic kidney disease. Cell Signal. 2024;124:111413. doi:10.1016/j.cellsig.2024.111413.
[41] Maksimowski N, Williams VR, Scholey JW. Kidney ACE2 expression: implications for chronic kidney disease. PLOS One. 2020;15(10):e0241534. doi:10.1371/journal.pone.0241534.